国家电网
STATE GRID
中国电力科学研究院有限公司
CHINA ELECTRIC POWER RESEARCH INSTITUTE

IET The Institution of Engineering and Technology

WILEY

A R T I C L E C A T E G O R Y

Power frequency magnetic field interference suppression method for online frequency response analysis of power transformers

Yangchun Cheng[1,*] 🄳   **Xiangdong Liu**[2,*]   **Yufei Sha**[3] | **Wenzhi Chang** [4] **Jiangang Bi**[4]

[1] State Key Laboratory of Alternate Electrical Power System with Renewable Energy, North China Electric Power University, Beijing, 102206, China

[2] Beijing Key laboratory of High Voltage and EMC, North China Electric Power University, Beijing, 102206 China.

[3] State Grid Yancheng Power Supply Company, Yancheng, Jiangsu, 224005, China

[4] Institute of High-Voltage Technology, China Electric Power Research Institute, Beijing, 100192 China.

Correspondence
chych@ncepu.edu.cn

*These authors contributed equally to this work.

Abstract

Frequency response analysis is widely used for the offline diagnosis of winding deformations in power transformers. To apply it to a working transformer, the magnitude of signals of the response current, which is of the order of microamperes, needs to be measured by using Rogowski coil sensors against the load current of the order of thousands of amperes. The saturation of the power frequency magnetic field in current sensors must be inhibited to ensure the accurate measurement of response currents with such a small magnitude. The authors of this paper propose a method to suppress the power frequency magnetic field by using a sensing system involving a special connection of three-phase current sensors based on the rule that the sum of the three-phase power frequency load currents of the transformer is close to zero. Each sensor consists of two secondary-side coils: a measuring coil and an anti-saturation coil. The anti-saturation coils are connected in parallel with one anothes through small inductors to eliminate the power frequency magnetic field in the cores of the sensors. We use theoretical analysis to derive the solution to this system. The results of experiments to verify the proposed method showed that it enables the sensors to function with a transformer carrying a load current of 2333 A, while incurring a relative error in the response current that is smaller than 2%.

Index Terms—Condition monitoring; current sensor; frequency response analysis; magnetic field saturation; online detection; power transformer; windings deformation.

1 | INTRODUCTION

The transformer is the most important electrical equipment in power networks, and its safe operation is crucial for the power systems [1]. Defects in transformers need to be identified before they lead to accidents or failure [2]. Transformers encounter the problem of winding deformations due to deficiencies in their design, short-circuit resistance calculations, manufacturing and material selection for older models, as well as sudden short-circuit accidents in the transmission channel near the substation. When the transformer is subjected to a short-circuit current, its windings may be deformed because they cannot withstand the resulting electromagnetic force. A minor deformation can evolve into a large one under the impact of multiple instances of large currents [3], and deformed windings are significantly mechanically weaker than normal windings. Transformers with deformed windings are thus more likely to break down. According to the International Council on Large Electric Systems (CIGRE), one-third of all transformer failures are caused by winding deformations [4].

Many methods are available for the offline detection of winding deformations, and frequency response analysis (FRA) is the one most widely used in the power industry owing to its high sensitivity and accuracy [5], [6]. The Chinese power industry and the International Electrotechnical Commission (IEC) have proposed standards for the application of FRA [7], [8]. However, taking the transformer offline is problematic because of the high demand for electricity. Therefore, many researchers have investigated extending offline FRA to the online monitoring of the windings of the transformer [9], [10]. In past research, we proposed a method for injecting an excitation signal into a working transformer and measuring the signals of the response current by using Rogowski coil sensors [11]-[13].

However, power frequency load currents of the order of hundreds and even thousands of amperes run through the windings of the transformer. This current usually causes the magnetic core of the response current sensor used for FRA to become saturated, and this prevents it from measuring FRA signals. In previously reported experiments, we measured the FRA signals at a substation by using a coil-type current sensor. Only when the power frequency current crossed zero could the FRA signal be measured [11] in this case. This is clearly not a reliable solution.

In this paper, we propose a method to suppress the interference caused by the power frequency load current during measurements of the current signals for FRA, particularly the saturation of the magnetic field in the core of the sensors. We provide the basic principle and a theoretical

analysis of the proposed method, and verify its feasibility and accuracy through experiments.

2 PROBLEM OF MAGNETIC FIELD SATURATION IN CURRENT SENSOR DURING ONLINE FRA

2.1 Application scenario of current sensors for online FRA

Frequency response analysis is widely used for the offline diagnosis of winding deformations in power transformers. It involves considering the windings of the transformer as an inductance–capacitance network. The deformation of the windings leads to changes in the inductance and capacitance of the network, and, thus, the function of the network. For example, as shown in Figure 1, a swept frequency voltage U_i is applied to the high-voltage terminal of the C-phase winding of a transformer with three-phase windings by using a source of voltage U_S, and the response voltage U_o is measured at the neutral terminal. The amplitude of the transfer function H of the C-phase winding is calculated as U_o/U_i. If H is different from its original value, this means that the windings have been mechanically deformed. The frequency of U_i usually ranges from 1 kHz to 1 MHz.
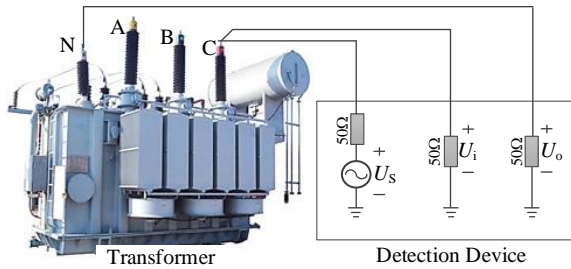

FIGURE 1. Measurement for the offline FRA of transformers

The principle above can be extended to online FRA. That is, the excitation signal is injected into and the response signal is measured on a working transformer. Furthermore, the network function of the windings is calculated by using the signals to diagnose winding deformations in the transformer. Of course, there are many differences between offline and online FRA. Because the windings in a working transformer have a high potential, it is difficult to measure signals of the response voltage on the windings. However, current sensors based on a Rogowski coil can be installed outside the high-voltage bushing to measure the response current on the windings. Therefore, the response currents (for FRA) are important signals for online FRA.
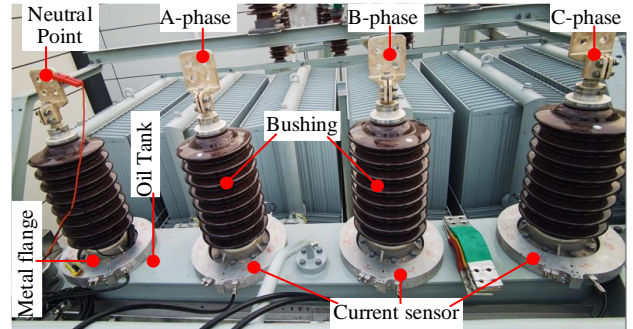
A typical scenario for the application of current sensors for FRA to an SSZ11-50000 kVA/110 kV transformer is shown in Figure 2, and was used for this study. When the excitation current I_S for FRA was injected into the neutral point N of the windings through a coil (called the excitation coil) by a

voltage source U_S, the response currents I_{AF1}, I_{BF1}, and I_{CF1} for FRA appeared in the high-voltage terminal of the three-phase windings and the three-phase bushings. The sensors used to measure the response current were installed on the oil tank of the transformer around the high-voltage bushings, and were thus at zero potential. The high voltage between the windings and the sensors was borne by the insulation of the bushing.

Before the transformer was connected to the power grid, we measured its response currents for FRA. The terminal of the windings of the A phase at 35 kV was grounded. When the peak amplitude of U_S was 4 V at 10 kHz, the induced voltage U_N at the neutral point N was 199.3 mV, and the output voltage U_{AF2} of the response current sensor around the A-phase bushing was 2.25 mV, as shown in Figure 3. The signal of the response current for FRA had a very small magnitude. We also confirmed the safety of this type of installation through experiments by the manufacturer of the transformer and at a power station [11]-[13].
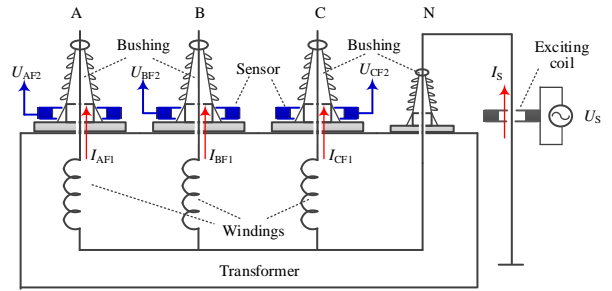
(a) Schematic circuit diagram

(b) Scenario of sensor installation (around 35 kV three-phase bushings and neutral-point bushing)

FIGURE 2. Scenario for the application of the current sensors for measurements for online FRA
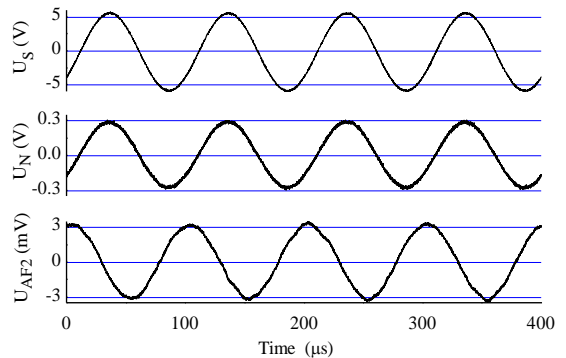

FIGURE 3. A result of current measurements for FRA (10 kHz)

The aim of online FRA is not to obtain the data (such as the transfer function H of the winding) online, as these are usually obtained through offline measurements. A comparison of the test settings for offline and online FRA in Figures 1 and 2, respectively, shows a significant difference between them. In case of offline FRA, the voltage transfer functions of single windings are obtained from the voltage signals and used as the criterion for diagnosis. In case of online FRA, the response current in one winding is affected by those in the other two-phase windings, the load of the transformer, and even the network of the power grid. Therefore, some form of a network function must be established based on the current signals. At the same time, a new diagnostic criterion is formulated based on a comparison with its previous value or that of the same type of winding. We have obtained preliminary results regarding this problem, and plan to present them in future work in the area.

2.2 Magnetic saturation of the current sensor

The current sensor converts the measured current I_1 into the output voltage U_2. The theory and structure of the Rogowski coil sensor are shown in Figure 4.

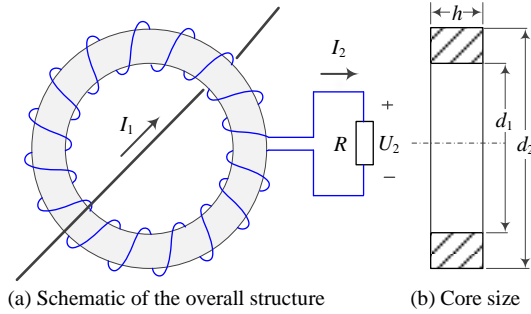(a) Schematic of the overall structure (b) Core size

FIGURE 4. Theory and structure of the Rogowski coil sensor

The theory of the Rogowski coil yields the following formulae:

$$j\omega M\dot{I}_1 = j\omega L\dot{I}_2 + \dot{U}_2 = j\omega L\dot{I}_2 + R\dot{I}_2 \tag{1}$$

$$L = Mn = \frac{\mu_0 \mu_r h n^2}{2\pi}\ln\frac{d_2}{d_1} \tag{2}$$

$$Z_C(j\omega) = \frac{\dot{U}_2}{\dot{I}_1} = \frac{j\omega MR}{j\omega L + R} \tag{3}$$

$$f_L = \frac{1}{2\pi}\frac{R}{L} \tag{4}$$

where j is the sign of the imaginary part of the expression, n is the number of turns of the coil, L is its inductance, M is the mutual inductance between the coil and the line bearing the measured current, I_1 is the measured current surrounded by the coil, I_2 is the current in the coil, R is its integral resistance, and U_2 is the output of the sensor. ω is the angular frequency of the signal, μ_r is the relative magnetic permeability of the material of the core of the coil, μ_0 is the permeability of vacuum, and h, d_1, and d_2 are the height, inner diameter, and outer diameter of the core of the coil,

respectively. Z_C is the transfer impedance of the sensor that describes the characteristics of its output, and f_L is its lower cutoff frequency. The small dot above each variable indicates that it is a phasor.

Figure 2 shows that the sensor was installed outside the root of the bushing. Its inner diameter needed to be sufficiently large to surround the bushing, while its height needed to be smaller than that of the metal flange of the bushing (smaller than 50 mm). According to (1)~(4), using a soft magnetic core with a large value of μ_r is the only way to obtain a range of frequency of 1 kHz~1 MHz while maintaining a large value of Z_C for a sensor with such a large diameter and limited cross-sectional area.

Our experience with offline FRA has shown that the response current for it has a very small magnitude, even lower than 1 mA, which necessitates a high Z_C. To strike a compromise between a low f_L and a high Z_C, we designed a core made of an iron-based amorphous material, with values of d_1 of 290 mm, d_2 of 350 mm, and h of 25 mm to construct the sensor for the 35 kV bushings of the SSZ11-50000 kVA/110 kV-type transformer. The number of turns of the coil of the sensor, n, was 150, and its integral resistance, R, was 330 Ω. The shape of the sensor is shown in Figure 2 and its transfer characteristics are shown in Figure 5.
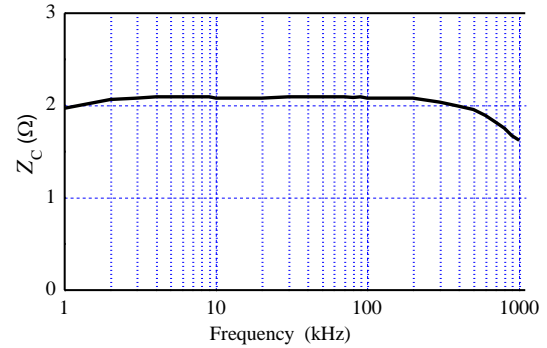

FIGURE 5. Transfer characteristics of the Rogowski current sensor

A wider frequency band than that in the range of 1 kHz~1 MHz is beneficial for diagnosing winding deformations. Although the characteristics of our sensor did not stay ideally constant in the range of 1 kHz~1 MHz, it yielded the best results for our design. Equations (1)~(4) show that if n is reduced, f_L increases, because of which signals close to 1 kHz cannot be accurately measured. If n is increased, the high cutoff frequency of the sensor decreases, because of which signals close to 1 MHz cannot be accurately measured due to the capacitance between the turns. Therefore, a magnetic core with a high permeability μ_r is an inevitable choice, and constitutes an important component of the sensor. Furthermore, field applications require open–close-type sensors, where this means that the core needs to be cut into two halves. The small gap between the parts drastically reduces the equivalent permeability of the core. According to our tests, the equivalent value of μ_r of the core at 50 Hz was reduced to about 3,000, although the material of the core had a permeability above 50,000.

The above analysis and tests showed that the magnetic core is the key component for ensuring the desired measurement band of the sensors. However, the FRA currents (called I_{AF1}, I_{BF1}, and I_{CF1} for the three phases, respectively, and generally referred to as I_{F1}) flow in the three windings, as do the power frequency load currents (called I_{AP1}, I_{BP1}, and I_{CP1} for the three phases, respectively, and generally referred to as I_{P1}) in a working transformer. The total currents I_{A1}, I_{B1}, and I_{C1} in the bushings are the superposition of the FRA currents and the power frequency load currents. As an example, the current in A-phase winding can be given as:

$$i_{A1}(t) = \sqrt{2} I_{AF1} \sin(\omega t) + \sqrt{2} I_{AP1} \sin(\omega_P t + \varphi_0) \quad (5)$$

where ω_P is the power angular frequency and φ_0 is the original phase angle of the load current. The rated power frequency load currents in normal transformers range from hundreds to thousands of amperes. For the SSZ11-50000 kVA/110 kV-type transformer, the rated values of I_{AP1} with 110 kV, 35 kV, and 10 kV windings were 262.4 A, 789.3 A, and 2749.3 A, respectively. Thus, the power frequency load currents were much larger than the FRA response current.

Such a large current inevitably leads to the saturation of the magnetic field of the core of the sensor. For example, the waveform of the output voltage U_{AP2} of the sensor shown in Figure 2 for a 50 Hz power current I_{AP1} appears to be clearly deformed, as shown in Figure 6. When I_{AP1} was 50 A, the waveform of U_{AP2} deviated slightly from the sinusoidal waveform, and its peak value was 28 V. In this case, the critical saturation current of the sensor was 50 A. Therefore, the normal load current of the transformer can cause the core of the sensor to become deeply magnetically saturated. This can lead to severe magnetostrictive vibrations that cause the sensor to fail. Furthermore, a large amount of power frequency noise occurs in the output of the sensor that poses serious difficulties in the design of the noise compression filter.
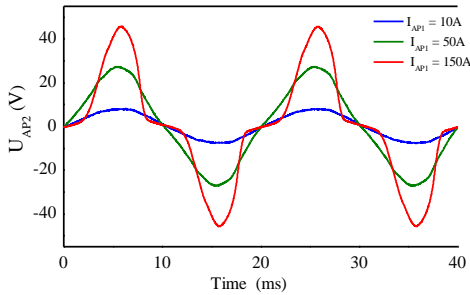

FIGURE 6. Output of the sensor to the power frequency current

2.3 Conventional methods to suppress saturation of magnetic field at the core of current sensor

Two kinds of methods are commonly used to suppress the saturation of the magnetic field in the core of the coil-type current sensor under the influence of a large power frequency current. The first involves reducing the magnetic permeability μ_r of the core by using a material with a low permeability, or by creating a gap in the path of the loop of the core. A magnetic core with a high permeability must be used to obtain the required measurement band in case of online FRA. This method to suppress the saturation of the magnetic field is clearly unfeasible here.

The second method involves using an inductive integral impedance. The resistance R is replaced by the parallel combination of R and the inductance Lc in (1)~(4) and Figure 4. The inductance L of the sensors shown in Figure 2 was 63 mH. Therefore, if the output voltage U_{AP2} is 5 V when the 50 Hz power current I_{AP1} is 500 A, the integral inductance Lc needs to be 4.785 mH. It is difficult to manufacture an inductor with this value because it must bear a large current of up to 3.33 A (this value increases proportionally when I_{AP1} is larger than 500 A), and it should have a low volume to facilitate field applications. Moreover, the lower cutoff frequency f_L of the sensor with this inductor is higher than 20 kHz ($\mu_r \approx 1600$ at frequency around 20 kHz), which is much larger than the required 1 kHz. Therefore, it is nearly impossible to suppress the power frequency noise while maintaining the required frequency band by using inductive integral impedance.

Thus, a new method to suppress the power frequency magnetic field in the core of the sensor is needed for the sensor to operate steadily and accurately.

3 | SUPPRESSING THE POWER FREQUENCY MAGNETIC FIELD

The magnetic field induced by the power frequency current significantly increases the difficulty of current measurement for online FRA. Below, we proposed a method to suppress it based on three-phase current sensors.

3.1 | Basic structure and principle

The maximum density of the magnetic flux B_{mag} under the power frequency in the core of a normal coil-type sensor can be calculated from (1) and (2) as follows:

$$B_{mag} = \sqrt{2} \frac{\mu_0 \mu_r \left| \dot{I}_1 - n\dot{I}_2 \right|}{\pi d_1} = \sqrt{2} \frac{\mu_0 \mu_r R I_1}{\pi d_1 \left| j\omega_P L + R \right|} \quad (6)$$

It is clear from the above that the basic principle of magnetic field suppression is to provide a sufficiently large secondary-side current I_2 by using a sufficiently small integral impedance or integral resistance R.

We use three current sensors for three-phase windings for online measurements of the FRA. In light of the large inductance Lc mentioned above, we assume that the sensors of the B and C phases can take the value of Lc of the sensor of phase A, as shown in Figure 7. The output ports of the sensors are connected in parallel with one another as well as being connected to the integral resistance R. The equivalent circuit is shown in Figures 7(b) and (c), in which the three-phase windings of the power transformer are represented by

the impedances Z_{WA}, Z_{WB}, and Z_{WC}, respectively. The power frequency electric potentials are represented by E_A, E_B, and E_C, the three-phase loads of the transformer are represented by Z_{LA}, Z_{LB}, and Z_{LC}, while the excitation voltage and the current for FRA are represented by U_S and I_S, respectively.

In case of balanced three-phase power frequency load currents, we have the following:

$$\dot{I}_{AP1} + \dot{I}_{BP1} + \dot{I}_{CP1} = 0 \tag{7}$$

Therefore,

$$\dot{I}_{AP2} + \dot{I}_{BP2} + \dot{I}_{CP2} = 0 = \dot{I}_{P2} \tag{8}$$

$$\dot{U}_{P2} = R\dot{I}_{P2} = 0 \tag{9}$$

We import (9) into (1) and (6) to obtain:

$$\dot{I}_{AP1} - n\dot{I}_{AP2} = 0 \quad , \quad B_{mag} = \sqrt{2}\frac{\mu_0\mu_r\left|\dot{I}_{AP1} - n\dot{I}_{AP2}\right|}{\pi d_1} = 0 \tag{10}$$
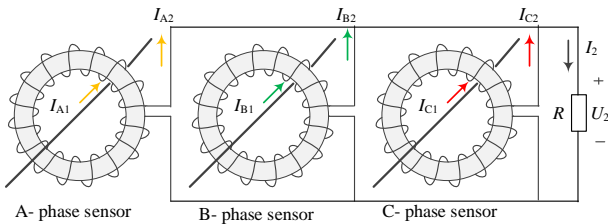
That is, the power frequency magnetic field in the cores of the sensors is zero such that the problem of magnetic saturation does not occur. In comparison with the conventional method based on integral impedance, the B-phase and C-phase sensors are the integral impedance L_c of the A-phase sensor in this structure, and vice versa. Given the principle underlying the construction of the conventional sensor, this integral impedance is too high to effectively suppress the power frequency magnetic field. However, in our proposed sensor system, the integral impedance is active, rather than passive, and thus has a source of induced potential in it from I_{BP1} and I_{CP1} that neutralizes the voltage when coupled with I_{AP1}. Therefore, it has different characteristics from those of the conventional sensor.

To simplify the description of the currents for FRA, we assume that the impedances Z_{WA}, Z_{WB}, and Z_{WC} are equivalent, as are the impedances Z_{LA}, Z_{LB}, and Z_{LC}. We then obtain the following:

$$\dot{I}_{AF2} = \dot{I}_{BF2} = \dot{I}_{CF2} = \dot{I}_{F2}/3 \tag{11}$$

$$\dot{U}_{F2} = R\left(\dot{I}_{AF2} + \dot{I}_{BF2} + \dot{I}_{CF2}\right) = \frac{R}{n}\left(\dot{I}_{AF1} + \dot{I}_{BF1} + \dot{I}_{CF1}\right) \tag{12}$$

That is, the response current for FRA can be accurately measured.

(a) Schematic of the structure of the three-phase sensor system

(b) Circuit topology under the power frequency current
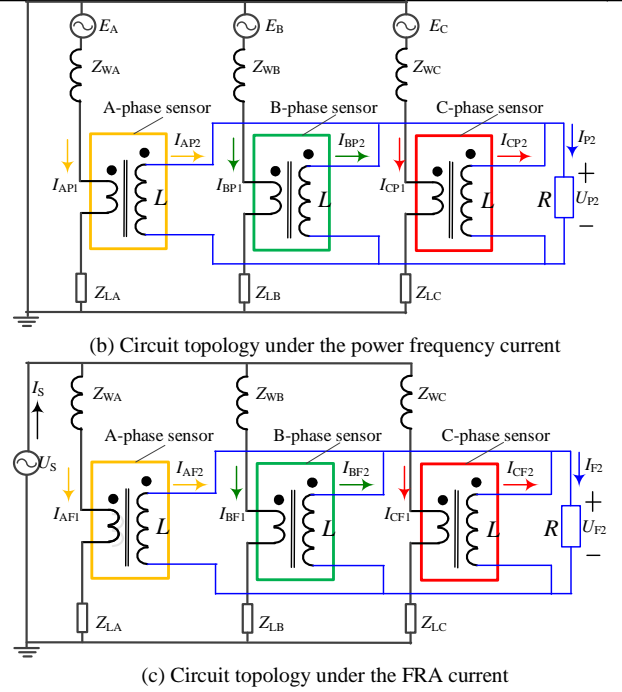

(c) Circuit topology under the FRA current

FIGURE 7. Principle of the method to suppress the power frequency magnetic field based on three phase sensors

3.2 | Improved structure and principle

It is clear from (12) that the measurement system shown in Figure 7 cannot distinguish among the response currents I_{AF1}, I_{BF1}, and I_{CF1}. Therefore, the three-phase windings of the power transformer are consider as a whole, rather than as three components. Deformations in the A-phase windings cannot be distinguished from those in the B-phase windings in this case. We thus propose an improved structure to be able to do so.

The improved structure is shown in Figure 8. The three sensors have identical structure and configuration, including the core, its turns, and integral resistance. Each sensor has two coils on the same magnetic core. One (No. 2) is called the measuring coil while the other (No. 3) is called the anti-saturation coil. The anti-saturation coils of these three sensors are connected in parallel, and three small impedances z_3 are connected in series at the output port of the anti-saturation coil.
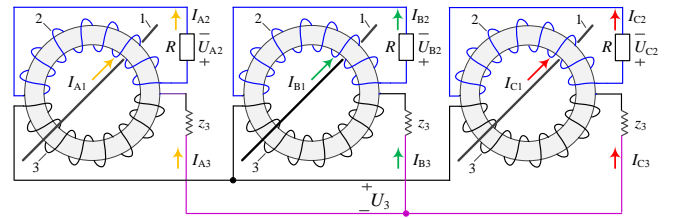
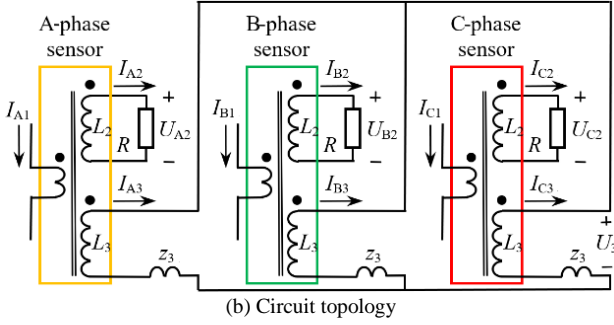
(a) Schematic of the structure

FIGURE 8. Improved method of suppression based on three phase sensors

When the sensor is considered to be a current transformer, the conductor (coil 1) in the bushing is the primary-side coil, and coils Nos. 2 and 3 are secondary-side coils. The circuit topology of the three phase sensors is shown in Figure 8(b), where I_{A1}, I_{B1}, and I_{C1} represent the total current on the windings of the three phases, I_{A2}, I_{B2}, and I_{C2} represent the total current on the measuring coils, and I_{A3}, I_{B3}, and I_{C3} represent the total current on the anti-saturation coils. The outputs of the total voltage of coil 2 are U_{A2}, U_{B2}, and U_{C2}, and are also the outputs of the sensors. Coil 3 has the same output as U_3.

The relationship among coils 1, 2, and 3 cannot be expressed by (1), and we need the corresponding original expressions of electromagnetic induction. Consider the A-phase sensor as an example:

$$R\dot{I}_{A2} = n_2 \frac{d\dot{\varphi}_A}{dt} = j\omega kn_2 \left(\dot{I}_{A1} - n_2 \dot{I}_{A2} - n_3 \dot{I}_{A3} \right) \quad (13)$$

$$\dot{U}_3 + z_3 \dot{I}_{A3} = n_3 \frac{d\dot{\varphi}_A}{dt} = j\omega kn_3 \left(\dot{I}_{A1} - n_2 \dot{I}_{A2} - n_3 \dot{I}_{A3} \right) \quad (14)$$

where n_2 is the number of turns of coil 2, n_3 is that of coil 3, φ_A is the magnetic flux in the core, and k is the coefficient of inductance:

$$k = L_2 / n_2^2 = L_3 / n_3^2 = \frac{\mu_0 \mu_r h}{2\pi} \ln \frac{d_2}{d_1} \quad (15)$$

where L_2 and L_3 are the inductances of coils 2 and 3, respectively. The corresponding formulae also hold for the sensors in phases B and C.

According to (5), the total current consists of the FRA current and the power frequency current. We now analyze these two kinds of current according to the principle of superposition.

3.3 Effect on the power frequency current

We consider only the power frequency current in the improved sensor system in this section, i.e., $I_{A1} = I_{AP1}$, $I_{A2} = I_{AP2}$, $\omega = \omega_P$, $I_2 = I_{P2}$, $U_{A2} = U_{AP2}$, and $U_3 = U_{P3}$, and so on B phase sensor and C phase sensor. According to the basic characteristics of the three-phase load balancing of the

electric power transmission system, we ideally have

$$\dot{I}_{AP1} + \dot{I}_{BP1} + \dot{I}_{CP1} = 0 \quad (16)$$

According to the circuit topology,

$$\dot{I}_{A3} + \dot{I}_{B3} + \dot{I}_{C3} = 0 \quad (17)$$

We combine (13) for the three phase sensors with (16) and (17) to obtain the following:

$$R \left(\dot{I}_{AP2} + \dot{I}_{BP2} + \dot{I}_{CP2} \right) = -j\omega_P kn_2^2 \left(\dot{I}_{AP2} + \dot{I}_{BP2} + \dot{I}_{CP2} \right) \quad (18)$$

The condition for (18) to hold is as follows:

$$\dot{I}_{AP2} + \dot{I}_{BP2} + \dot{I}_{CP2} = 0 \quad (19)$$

We then combine (14) for the three phase sensors with (16), (17), and (19) to obtain the following:

$$\dot{U}_{P3} = 0 \quad (20)$$

Then,

$$B_{mag} = \sqrt{2} \frac{\mu_0 \mu_r \left| \dot{I}_{AP1} - n_2 \dot{I}_{AP2} - n_3 \dot{I}_{AP3} \right|}{\pi d_1} \quad (21)$$

$$= \sqrt{2} \frac{\mu_0 \mu_r \left| z_3 \dot{I}_{AP3} \right|}{\pi d_1 \omega_P kn_3} \approx 0$$

where z_3 is a small impedance of the order of μH. Furthermore,

$$\dot{U}_{AP2} = R\dot{I}_{AP2} = n_2 \frac{d\dot{\varphi}_{AP}}{dt} \approx 0 \quad (22)$$

For the ideal condition in which the windings and loads of the three phases are balanced under a power frequency, the circuit topology in Figure 8(b) can be simplified into the circuit show in Figure 9(a) because $U_{P3} = 0$. If n_2 and n_3 are equal, the integral impedance of coils 2 and 3 can be connected together directly and in parallel, as shown in Figure 9(b). Clearly, there is a weak power frequency magnetic field in the core of the sensor because of the small impedance z_3.

Therefore, the magnetic field in the cores of the sensors is close to zero because the sum of the three-phase power frequency currents is zero. Thus, the power frequency magnetic field does not become saturated.
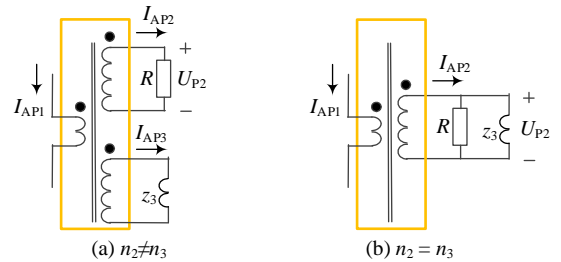

FIGURE 9. Equivalent circuit to the power frequency current

3.4 Effect on FRA current

We consider only the FRA currents in the improved sensor system in this section, i.e., $I_{A1} = I_{AF1}$, $I_{A2} = I_{AF2}$, $I_2 = I_{F2}$, $U_{A2} = U_{AF2}$, and $U_3 = U_{F3}$, and so on B phase sensor and C phase

sensor.

By combining (13) for the three phase sensors with (17), we obtain:

$$\dot{I}_{AF2} + \dot{I}_{BF2} + \dot{I}_{CF2} = \frac{j\omega k n_2}{R + j\omega k n_2^2}\left(\dot{I}_{AF1} + \dot{I}_{BF1} + \dot{I}_{CF1}\right) \tag{23}$$

Combining (14) for the three phase sensors with (17) yields:

$$3\dot{U}_{F3} = j\omega k n_3\left[\dot{I}_{AF1} + \dot{I}_{BF1} + \dot{I}_{CF1} - n_2\left(\dot{I}_{AF2} + \dot{I}_{BF2} + \dot{I}_{CF2}\right)\right] \tag{24}$$

Therefore,

$$\dot{U}_{F3} = \frac{j\omega k n_3 R}{3R + 3j\omega k n_2^2}\left(\dot{I}_{AF1} + \dot{I}_{BF1} + \dot{I}_{CF1}\right) \tag{25}$$

$$\dot{I}_{AF2} = \frac{j\omega k n_2 z_3 \dot{I}_{AF1} + j\omega k n_2 n_3 \dot{U}_{F3}}{j\omega k n_2^2 z_3 + j\omega k n_3^2 R + z_3 R} \tag{26}$$

Then, let

$$a = \frac{j\omega k n_2 z_3}{j\omega k n_2^2 z_3 + j\omega k n_3^2 R + z_3 R} \tag{27}$$

$$b = \frac{j\omega k n_2 n_3}{j\omega k n_2^2 z_3 + j\omega k n_3^2 R + z_3 R} \times \frac{j\omega k n_3 R}{3R + 3j\omega k n_2^2} \tag{28}$$

We then obtain

$$\begin{bmatrix} \dot{U}_{AF2} \\ \dot{U}_{BF2} \\ \dot{U}_{CF2} \end{bmatrix} = R\begin{bmatrix} \dot{I}_{AF2} \\ \dot{I}_{BF2} \\ \dot{I}_{CF2} \end{bmatrix} = R\begin{bmatrix} a+b & b & b \\ b & a+b & b \\ b & b & a+b \end{bmatrix} \cdot \begin{bmatrix} \dot{I}_{AF1} \\ \dot{I}_{BF1} \\ \dot{I}_{CF1} \end{bmatrix} \tag{29}$$

Then,

$$\begin{bmatrix} \dot{I}_{AF1} \\ \dot{I}_{BF1} \\ \dot{I}_{CF1} \end{bmatrix} = \frac{1}{R} \cdot \begin{bmatrix} a+b & b & b \\ b & a+b & b \\ b & b & a+b \end{bmatrix}^{-1} \cdot \begin{bmatrix} \dot{U}_{AF2} \\ \dot{U}_{BF2} \\ \dot{U}_{CF2} \end{bmatrix} \tag{30}$$

Clearly, the FRA currents I_{AF1}, I_{BF1}, and I_{CF1} can be calculated by the outputs of the set of sensors provided that the impedance matrix with respect to a and b is known. Equation (30) holds only if a is not equal to zero (in other words, if z_3 is not equal to zero).

Furthermore, if the frequency band of the sensor ranges from 1 kHz to 1 MHz (that is, RI_2 is much smaller than $j\omega LI_2$ in (1)), the sensor can be considered to be an ideal transformer. We then have,

$$\dot{I}_{AF1} = n_2\dot{I}_{AF2} + n_3\dot{I}_{AF3} \tag{31}$$

The circuit in Figure 8(b) is replotted in Figure 10 based on the equivalent circuit of the ideal transformer with respect to the A-phase sensor and the measured current I_{AF1} (this is similar to when the circuit is replotted with respect to the B-phase sensor or the C-phase sensor). In Figure 10, I^*_{AF1} is the converted value of I_{AF1} based on the numbers of turns of the primary-side coil and coil 2 (that is, $I^*_{AF1} = I_{AF1}/n_2$), and I^*_{AF3} is the converted value of I_{AF3} based on the numbers of turns of coils 2 and 3 (that is, $I^*_{AF3} = I_{AF3} \times n_3/n_2$). Our simulation-based analysis revealed that the impedances of the windings

and load of the transformer were considerably higher than the integral resistance R of the sensors in the range of frequency of the FRA. Therefore, the primary side of the B-phase and C-phase sensors constituted an open circuit. The integral resistance R and small impedances z_3 of the B-phase sensor were in parallel with those of the C-phase sensor, and were in series with the small impedance z_3 of the A-phase sensor. Compared with the second conventional method (Section 2.3) to suppress saturation based on an integral inductance (Lc) of 4.785 mH (which caused the lower cutoff frequency f_L of the sensor to increase to a value significantly higher than 20 kHz), the resistances R of the B-phase and C-phase sensors increased the impedance of coil 3 of the A-phase sensor. Thus, the A-phase sensor still had a small value of the lower cutoff frequency f_L, even though the impedance z_3 was much lower than 4.785 mH.
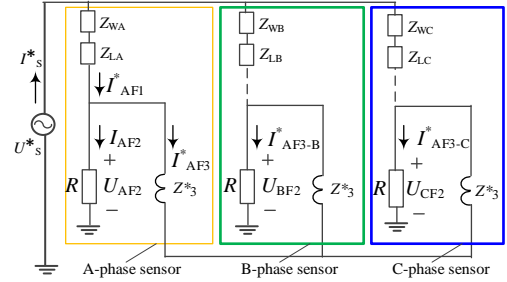

FIGURE 10. Equivalent circuit to the FRA current with respect to the A-phase sensor

3.5 Application based on actual sensors

We now detail the basic principle of the proposed method of suppression in the above context based on the idealized hypothesis. We consider the complex conditions encountered applications.

Equations (23) and (24) come from (13) and (14). The leakage-induced inductance between coils 1 and 2, and between coils 1 and 3 is not considered in (13) and (14). This inductance is related to the manufacturing of the sensors, and is different for each. Moreover, the coefficient k is related to the value of μ_r of the core of the sensor, and μ_r is in turn related to the frequency of the current, which is different for each core. It is thus difficult to theoretically determine an accurate value of the coefficient matrix in (29).

We hypothesize the following in the above derivation: Each of the three phase sensors has the same number of turns of coils 2 and 3, integral resistance R, and serial impedance z_3. These parameters may differ between sensors in applications.

Equation (29) can be extended to a more general form by considering the leakage inductance, the complex value of μ_r of the core of the sensor, and differences in the values of parameters among the three phase sensors as shown in (32):

$$\begin{bmatrix} \dot{I}_{AF1} \\ \dot{I}_{BF1} \\ \dot{I}_{CF1} \end{bmatrix} = \begin{bmatrix} Z_{AA} & Z_{AB} & Z_{AC} \\ Z_{BA} & Z_{BB} & Z_{BC} \\ Z_{CA} & Z_{BC} & Z_{CC} \end{bmatrix}^{-1} \cdot \begin{bmatrix} \dot{U}_{AF2} \\ \dot{U}_{BF2} \\ \dot{U}_{CF2} \end{bmatrix} \tag{32}$$

where each element of the above impedance matrix is defined as in (33) and (34). For instance,

$$Z_{\mathrm{AA}} = \left. \frac{\dot{U}_{\mathrm{AF2}}}{\dot{I}_{\mathrm{AF1}}} \right|_{i_{\mathrm{BF1}}=i_{\mathrm{CF1}}=0} \tag{33}$$

$$Z_{\mathrm{AB}} = \left. \frac{\dot{U}_{\mathrm{AF2}}}{\dot{I}_{\mathrm{BF1}}} \right|_{i_{\mathrm{AF1}}=i_{\mathrm{CF1}}=0} \tag{34}$$

Equation (32) is theoretically grounded in a passive multi-port circuit network, the details of which are not described here because of limited pages.

Equation (32) then describes the characteristics (relationship between the input and output) of the three-phase sensor system. Considering the above-mentioned uncertainties, the parameters of the impedance matrix at each frequency can be determined through laboratory calibration tests according to (33) and (34).

4 EXPERIMENTAL VERIFICATION

4.1 Setup of the verification experiment

Our experiments to test the proposed method involved three sensors connected to one another according to the topological structure shown in Figure 8. The details of the sensors have been provided in Section 2. Coils 2 and 3 both had 150 turns, z_3 was an inductor with an inductance of 100 μH, and a power frequency current generator was used to produce three-phase currents of up to 500 A. The FRA current was generated by a signal generator. The outputs of the sensors were recorded by a digital oscilloscope. This experimental scenario is shown in Figure 11.
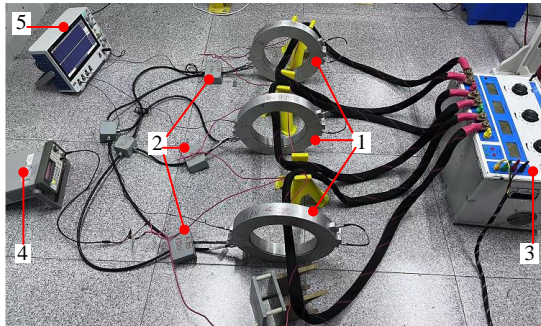
1-sensors; 2-inductor z_3; 3-power frequency current generator; 4-high-frequency signal generator; 5-digital oscilloscope

FIGURE 11. Experimental setup

4.2 Suppression of power frequency magnetic field

Large, three-phase power frequency currents were supplied to the primary side of the three phase sensors, and a high-frequency FRA current was provided to the A-phase sensor.

Some outputs of the sensors are shown in Figures 12 and 13. It is clear that the outputs were the superposition of power frequency signals and high-frequency FRA signals. The peak value of each of the power frequency signals (U_{AP2}, U_{BP2}, U_{CP2}) shown in Figure 13 was approximately 6 V, and corresponded to a current of 500 A on the primary side. It is clear from the waveform of the power frequency signals that the sensors were far from being saturated under a power frequency current of 500 A. According to the ratio of the output of the sensor to the load current on the primary side, the latter reached a value of 2333 A if the power frequency signal in the output was 28 V (which means that the sensor had just begun being saturated, as shown in Figure 6). Therefore, when the three sensors were connected according to the method illustrated in Figure 8, their magnetic cores were not saturated even when the load of the transformer was as high as 2333 A.

It was easy to eliminate the several volts of power frequency interference in the output signals of the sensors by using a normal electronic filter, as shown in Figure 12(c).
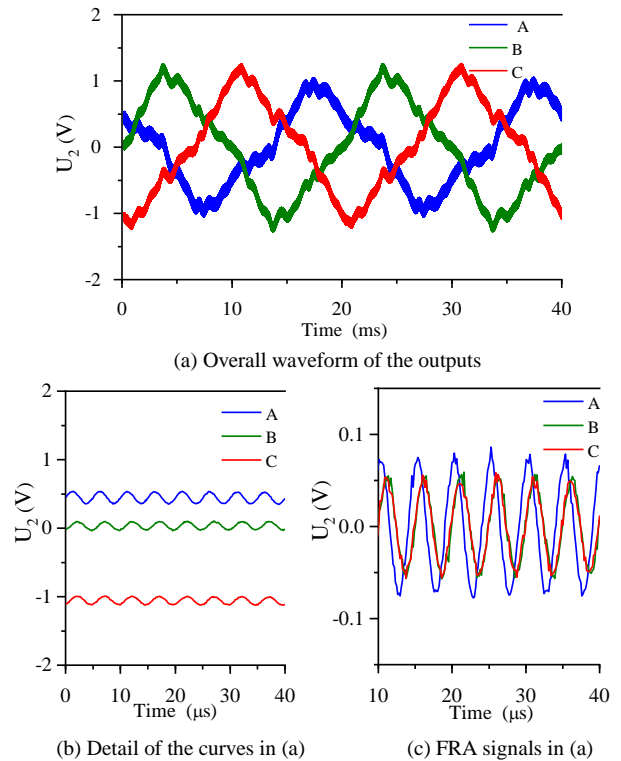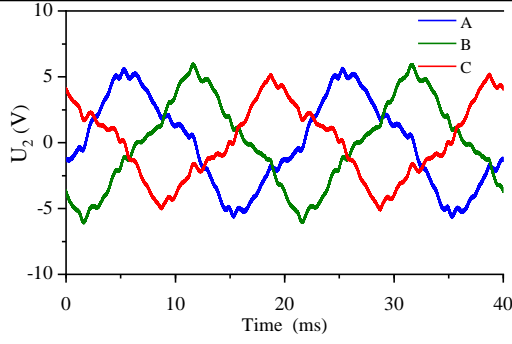

(a) Overall waveform of the outputs

(b) Detail of the curves in (a)

(c) FRA signals in (a)

FIGURE 12. Superimposed output signals of the three phase sensors under a 50 Hz current of 100 A and an FRA current of 200 kHz

FIGURE 13. Superimposed output signals of the three phase sensors under a 50 Hz current of 500 A and an FRA current of 200 kHz

4.3   Calibration of the sensing system

Before measuring the FRA current, the three-phase sensor system needed to be calibrated to obtain the parameters of the impedance matrix. The circuit configuration shown in Figure 11 was used to carry out the calibration experiments, except that the power frequency circuit was disconnect to eliminate its influence.

The value of each of I_{AF1}, I_{BF1}, and I_{CF1} was set to 70.72 mA to measure U_{AF2}, U_{BF2}, and U_{CF2}, and to then calculate the impedance matrix in the range of FRA frequencies of 1 kHz~1 MHz, at representative frequency points according to (33) and (34). One set of the outputs of the sensor is shown in Figure 14, and corresponds to $I_{AF1} = 70.72$ mA, $I_{BF1} = I_{CF1} = 0$ mA, and $\omega = 2\pi \times 400$ kHz. Among the outputs, $U_{AF2} > U_{BF2} = U_{CF2}$.

Having obtained U_{AF2}, U_{BF2}, and U_{CF2}, the value of each element in the impedance matrix was calculated by using (33) or (34). The amplitude and angle of elements in the first line of the impedance matrix are shown in Figure 15, while those of elements in its second and third lines were similar to those of the first line.
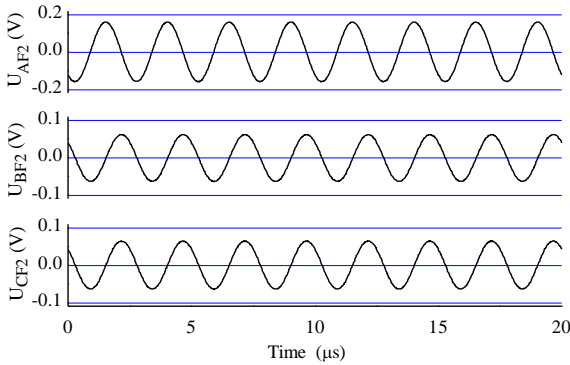
FIGURE 14. Outputs of the three phase sensors under an FRA current of 400 kHz in phase A
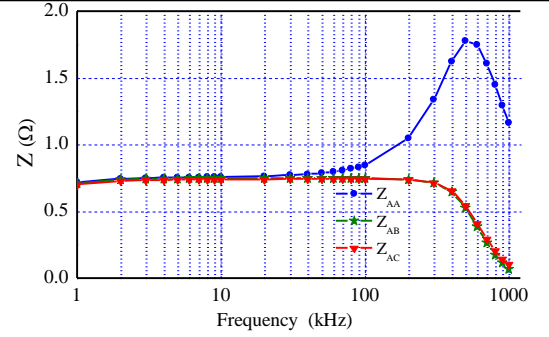

(a) Amplitude of the impedances
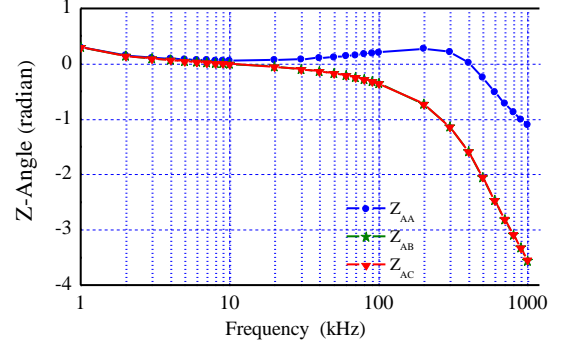
(b) Angles of the impedances

FIGURE 15. Values of elements in the first line of the impedance matrix

4.4   Solving for the FRA response current

The accuracy of the sensing system used to measure the FRA current was verified through experiments. We set I_{AF1}, I_{BF1}, and I_{CF1} to 56.58 mA one by one as the FRA current. They were then calculated from the outputs of the sensing system, and the results were compared with real values of the FRA currents. The relative error (ratio of the absolute error to the real values of I_{AF1}) between the calculated values of I_{AF1}, I_{BF1}, and I_{CF1}, and their real values of $I_{AF1} = 56.58$ mA, and $I_{BF1} = I_{CF1} = 0$ were below 5% as shown in Figure 16. The relative errors in most frequency bands were even smaller than 1%. When the FRA current was applied to the B phase or the C phase, the results were similar to those for the A phase.
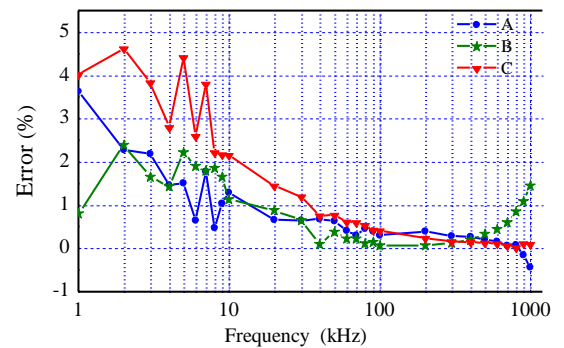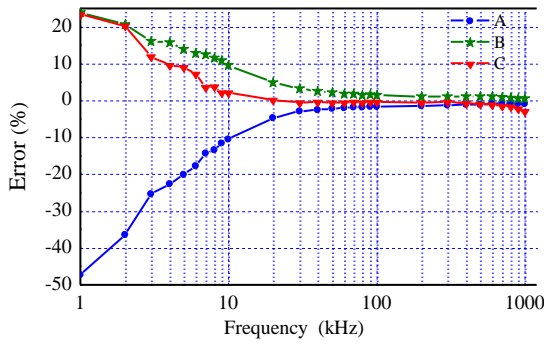

FIGURE 16. Relative errors of the three-phase sensing system in measuring the FRA current when $I_{AF1} = 56.58$ mA, and $I_{BF1} = I_{CF1} = 0$

When the same FRA current of 70.72 mA as above was

synchronously applied to phases A and B, the relative errors between their calculated and real values were smaller than 5% in most frequency bands, as shown in Figure 17. When this value of the FRA current was synchronously applied to phases A, B, and C, the relative errors were still smaller than 5% in the major frequency bands as shown in Figure 18. The overall relative error of the sensing system was smaller than 2% in the range of frequencies from 60 kHz to 800 kHz.
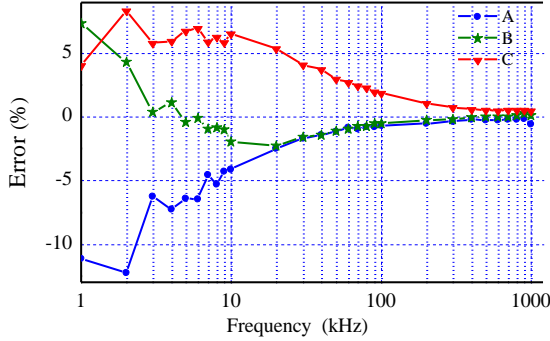
FIGURE 17. Relative error between the real FRA current and its value measured by the three-phase sensing system when $I_{AF1} = I_{BF1} = 56.58$ mA, and $I_{CF1} = 0$

FIGURE 18. Relative error between the real FRA current and its values measured by the three-phase sensing system when $I_{AF1} = I_{BF1} = I_{CF1} = 56.58$ mA.

5 DISCUSSION

5.1 Function of z_3

The function of z_3 is displayed in (27)~(29). If $z_3 = 0$, then $a = 0$, the element in the impedance matrix has the same value, and it has no inverse matrix. Therefore, the FRA current cannot be obtained by the outputs of the sensing system. Hence, the function of z_3 ensures that the matrix is invertible. In other words, it ensures that the sensor in one phase has different outputs from the FRA response current in the same phase as well as that in another phase. For example, U_{AF2} has different values to I_{AF1} and I_{BF1}. z_3 should be set to be sufficiently large to ensure this difference. Therefore, the sensing system can distinguish among I_{AF1}, I_{BF1}, and I_{CF1}.

However, z_3 determines the magnetic flux of the power frequency B_{mag} in the core of the sensors by using (21). To reduce B_{mag} as much as possible, z_3 should be set to a very small value. In sum, z_3 should be sufficiently small at the given power frequency and sufficiently large in the range of frequency of the FRA. An inductor is a good choice for z_3. This inductor should be able to handle a large power frequency current (up to I_{AP1}/n_3, perhaps several or tens of amperes).

z_3 was set to 100 µH in our experiments. This corresponds to a power frequency saturation-inducing current of the sensing system of 2333 A. A smaller z_3 yields a smaller U_{P2} and, thus, a larger saturation current. Because U_2 is the superposition of U_{P2} and U_{F2}, and a small value of U_{P2} is important to distinguish U_{F2} from U_2. If U_{P2} is 30 V, it cannot be eliminated by using commonly used active filters because it exceeds the range of input of the active filters.

The disadvantage of a smaller value of z_3 is that it makes it difficult to distinguish between elements of the impedance matrix. Figure 15 shows that the difference in impedance among the three phases was very small below 60 kHz. In this case, the relative error in the range of 1 kHz to 60 kHz was larger than that in the range of 60 kHz to 1 MHz, as shown in Figures 16~18. Therefore, the higher the value of z_3 is, the higher is the accuracy of the sensing system.

5.2 Analysis of effects under non-ideal conditions

Non-ideal situations may be encountered when suppressing the power frequency magnetic field in the cores of the sensors in the application of FRA on a live transformer. First, the values of μ_r of the cores of the three phase sensors are different from one another because of the process of cutting the material of the core. Therefore, the coefficient of inductance k of each sensor is different. This difference has a prominent effect on the outputs of the sensors at the power frequency. In this case, U_{P2} is non-zero even if z_3 is zero. Fortunately, the difference in the values of μ_r has a minor influence on the characteristics of transfer of the sensors in most ranges of frequency used for FRA because ωL is much larger than R in (3).

Second, the sum of the three-phase power frequency currents of the transformer is ideally equal to zero, as shown in (16). However, the actual sum of the currents invariably has a small value that is close to zero. By ignoring the impedance of z_3 at the power frequency, the following formula for the excitation current I_m of the magnetic field in a sensor can be deduced by using (14) and (25):

$$\dot{I}_m = \dot{I}_{AP1} - n_2 \dot{I}_{AP2} - n_3 \dot{I}_{AP3}$$
$$= \frac{R\left(\dot{I}_{AP1} + \dot{I}_{BP1} + \dot{I}_{CP1}\right)}{3R + 3j\omega_p L} \approx \frac{1}{3}\left(\dot{I}_{AP1} + \dot{I}_{BP1} + \dot{I}_{CP1}\right) \tag{35}$$

The degree of imbalance in the load current of the transformer in a power transmission grid is typically lower

than 3% of its value. The influence of this unbalanced current with respect to the power frequency magnetic flux in the core of the sensors is identical to that in a conventional sensor (which is shown in Figure 6). Given that the actual load of a transformer is usually smaller than 50% of its rated load, the maximum unbalanced current (3%) in the 10 kV windings is 41.24 A. According to (35), the magnetic flux caused by an unbalanced load current of 41.24 A in the cores of sensors in the three-phase sensing system is equal to that caused by a load current of 13.75 A in the core of a single conventional sensor. Therefore, the unbalanced load current of the SSZ11-50000 kVA/110 kV-type transformer cannot cause the core of the three-phase sensing system to become saturated.

6   CONCLUSION

The authors of this study proposed a method to suppress the power frequency magnetic field in the cores of the sensors in the application of FRA on living transformers based on the basic rule that the sum of the three-phase power frequency load currents is close to zero. The proposed method consists of a sensing system with a special connection among three phase current sensors. Unlike the conventional method to this end, this sensing system can drastically suppress the power frequency magnetic field in the cores of the sensors under large load currents of the transformer while maintaining the frequency band required for FRA.

The proposed three-phase sensing system increases the power frequency load current that can cause magnetic saturation in the core of the sensor from 50 A (in conventional methods) to 2333 A.

The FRA currents in the windings in the three phases can be calculated by using the outputs of the three-phase sensing system. The relative error in its calculations was found to be smaller than 2% in the range of frequencies from 60 kHz to 800 kHz.

ORCID

Yangchun Cheng   0000-0002-9002-4924
Xiangdong Liu   0000-0002-5638-9284
Yufei Sha   0000-0002-5005-3640
Wenzhi Chang   0000-0001-9642-5131
Jiangang Bi   0000-0003-0278-2029

REFERENCES

[1] Arputhasamy Joseph Amalanathan, Ramanujam Sarathi, Swayam Prakash, Ashok Kumar Mishra, Ribhu Gautam, Ravikrishnan Vinu, "Investigation on thermally aged natural ester oil for real-time monitoring and analysis of transformer insulation," *High Volt.*, vol. 5. no. 2, pp. 209 –217, Apr. 2020.

[2] Md Mominul Islam ; Gareth Lee ; Sujeewa Nilendra Hettiwatte, "Application of Parzen Window estimation for incipient fault diagnosis in power transformers," *High Volt.*, vol. 3. no. 4, pp. 303-309, Dec. 2018.

[3] Rafael M.R. Barros, Edson G. da Costa, Jalberth F. Araujo, Filipe L.M. de Andrade, Tarso V. Ferreira, "Contribution of inrush current to mechanical failure of power transformers windings," *High Volt.*, vol. 4. no. 4, pp. 300 –307, Dec. 2019.

[4] Zhongyong Zhao, Chenguo Yao, Chengxiang Li, and Syed Islam, "Detection of power transformer winding deformation using improved FRA based on binary morphology and extreme point variation," *IEEE Transactions On Industrial Electronics*, vol. 65, no. 4, pp. 3509–3519, April 2018.

[5] Steven D. Mitchell, James S. Welsh, "Methodology to locate and quantify radial winding deformation in power transformers", *High Voltage*, vol. 2, iss. 1, pp. 17–24, March 2017.

[6] J. C. Gonzales and E. E. Mombello, "Fault interpretation algorithm using frequency-response analysis of power transformers," *IEEE Trans. Power Del.*, vol. 31, no. 3, pp. 1034–1042, June 2016.

[7] *Frequency-response analysis on Winding Deformation of Power Transformers*, People's Republic of China, Electric Power Industry Standard, DL/T911-2004, ICS27.100, F24, Document No. 15182-2005 (in Chinese), 2005.

[8] *Measurement of Frequency Response*, IEC Standard 60076-18, Ed. 1.0, 2012-07, 2012.

[9] M. Bagheri, M. S. Naderi, and T. Blackburn, "Advanced transformer winding deformation diagnosis: moving from off-line to on-line," *IEEE Trans. Dielect. Elect. Insul.*, vol. 19, no. 6, pp. 1860–1870, December 2012.

[10] Chenguo Yao, Zhongyong Zhao, Yu Chen, Xiaozhen Zhao, Zhaojiong Li, Yong Wang, Zehong Zhou, and Gang Wei, "Transformer winding deformation diagnostic system using online high frequency signal injection by capacitive coupling," *IEEE Transactions on Dielectrics and Electrical Insulation,* vol. 21, no. 4, pp. 1486–1492, August 2014.

[11] Yangchun Cheng，Jiangang Bi，Wenzhi Chang，Yuan Xu，Xiaohua Pan，Xianwei Ma，Shuai Chang，" Proposed methodology for online Frequency-response analysis based on magnetic coupling to detect winding deformations in transformers，"High Volt.，vol. 5.no 3，pp.343-349，Jun.2020.

[12] Yangchun Cheng, Xiaohua Pan Wenzhi, Chang, and Jiangang Bi, "Analysis of the influence of outside equipment on the online deformation detection of transformers," in *Proc. 2016 IEEE International Conference on High Voltage Engineering and Application*, Chengdu, China, 2016, P-5-15.

[13] Yanghcun Cheng, Wenzhi Chang, Jiangang Bi, and Xiaohua Pan, "Signal injection by magnetic coupling for the online FRA of transformer winding deformation diagnosis," in *Proc. 1st International Conference on Dielectrics*, Montpellier, France , July 2016. pp. 905–908.